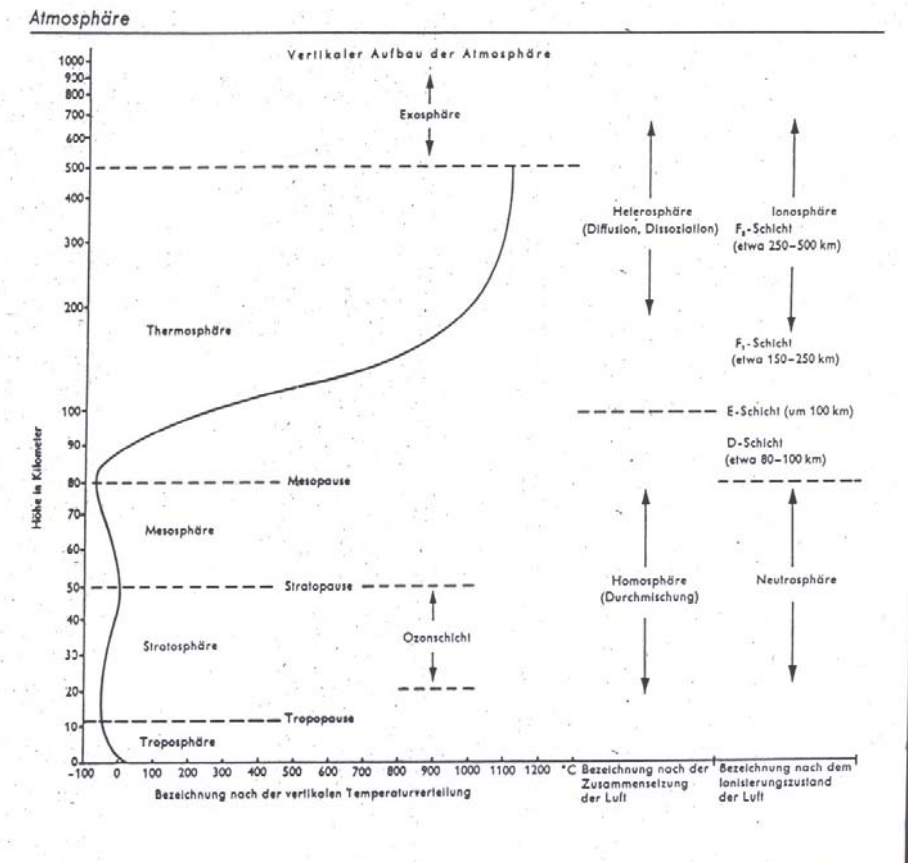

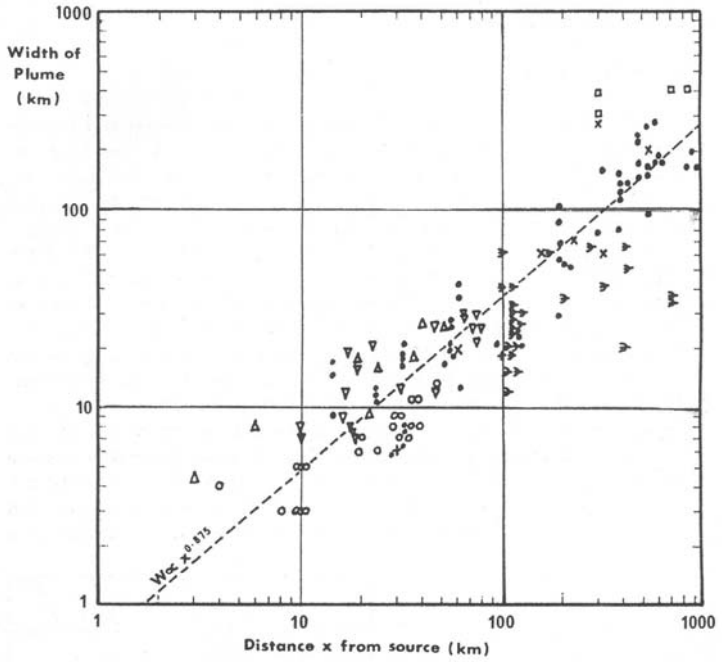

Figure 3.1.3: Data on the width of plumes as a function of distance
* Richardson and Proctor (1925) ∇ Porton data (Pasquill, 1974)
\+ Gifford (see Slade, 1968) • Classified project (ibid.)
Δ Braham *et al*., (1952) o Smith and Heffernan (1956)
• Mount Isa data (Biggs et *al*., 1978); Carras and Williams, (1981)
∋ Crabtree (1982): data collected over sea.

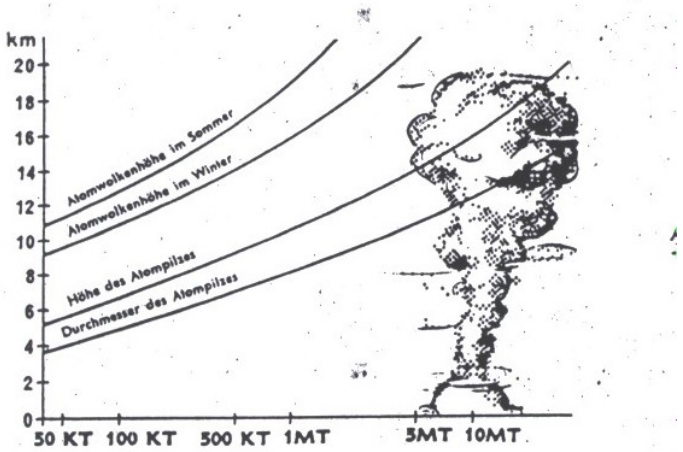

Abb. 6 Atompilzentwicklung und Sprengleistung

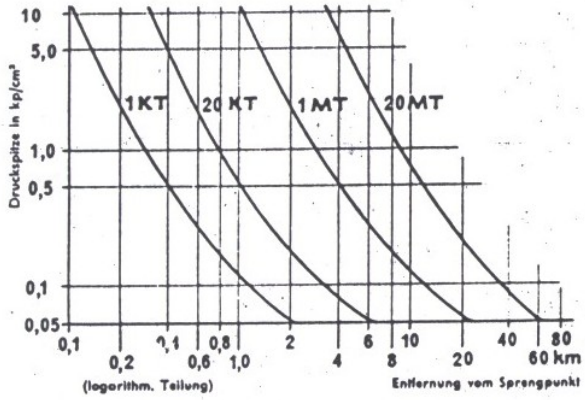

Abb. 7 Druckwirkung von Kernwaffen

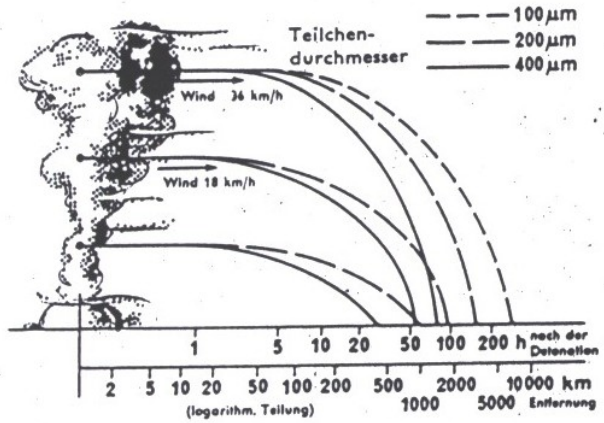

Abb. 8 Reichweite des radioaktiven Fallouts einer 10-Mt-Bombe

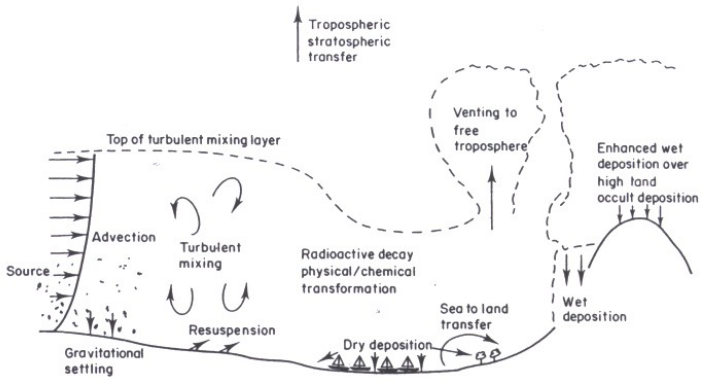

Figure 3.1 Schematic diagram of processes influencing radionuclides in the atmosphere.

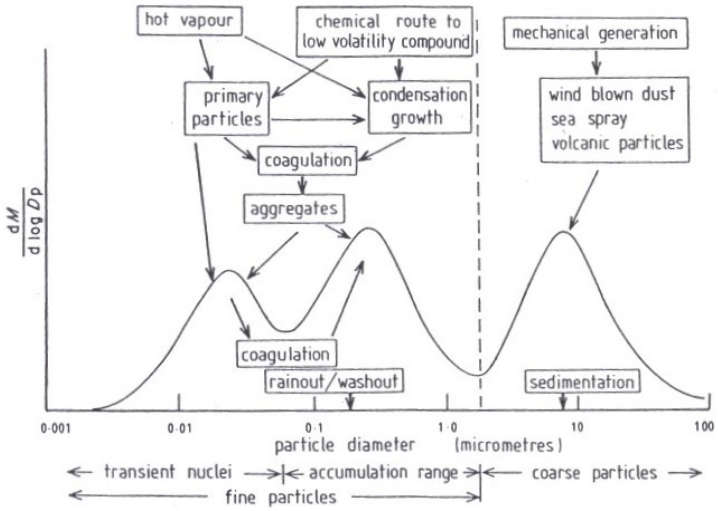

Figure 3.2 Schematic diagram of the size distribution (expressed as mass per increment in log particle diameter) and formation mechanisms for atmospheric aerosols (adapted from Harrison, 1990).

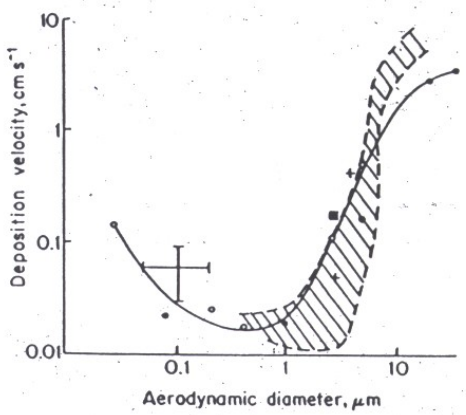

Figure 3.3 Experimental data from several sources, on deposition of small particles to grass. The symbols and hatched area represent the distribution of field and wind-tunnel data. (Copyright AEA.)

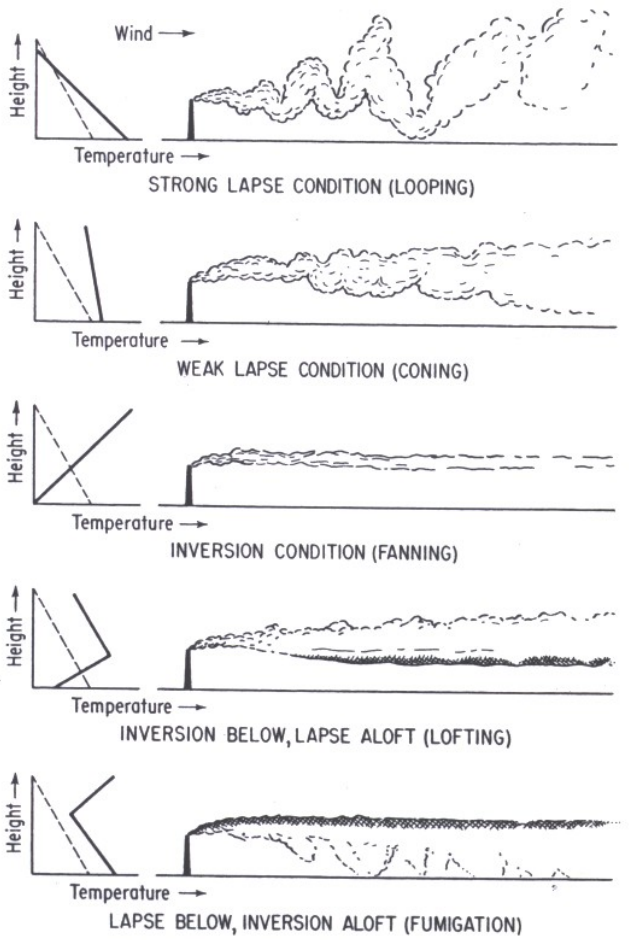

FIGURE 4-5 Schematic representation of stack-gas behavior under various conditions of vertical stability. Actual temperature (solid line) and dry adiabatic lapse rate (dashed line) are shown. [From U.S. Weather Bureau (1955).]

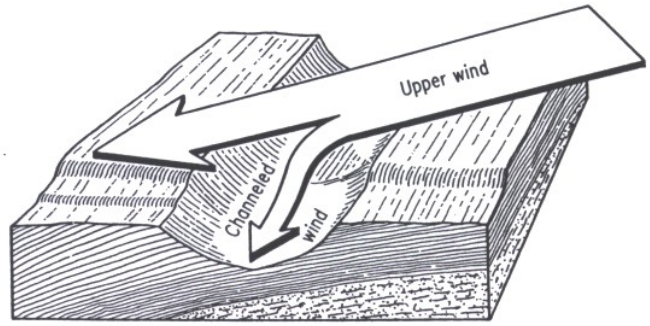

FIGURE 4-13 Wind channeling by valley walls. [From U.S. Weather Bureau (1955).]

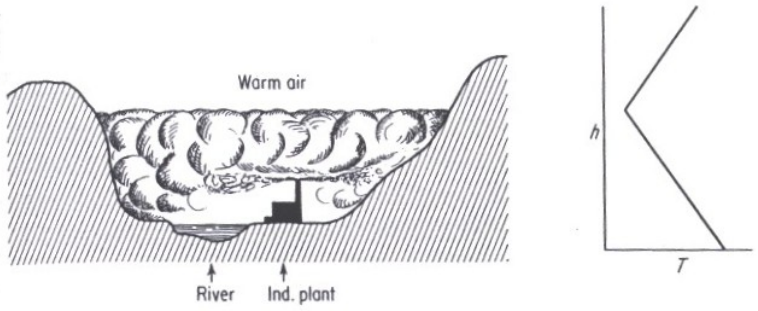

FIGURE 4-14 Fumigation of valley floor caused by an inversion layer that restricts diffusion from a stack. [From U.S. Weather Bureau (1955).]

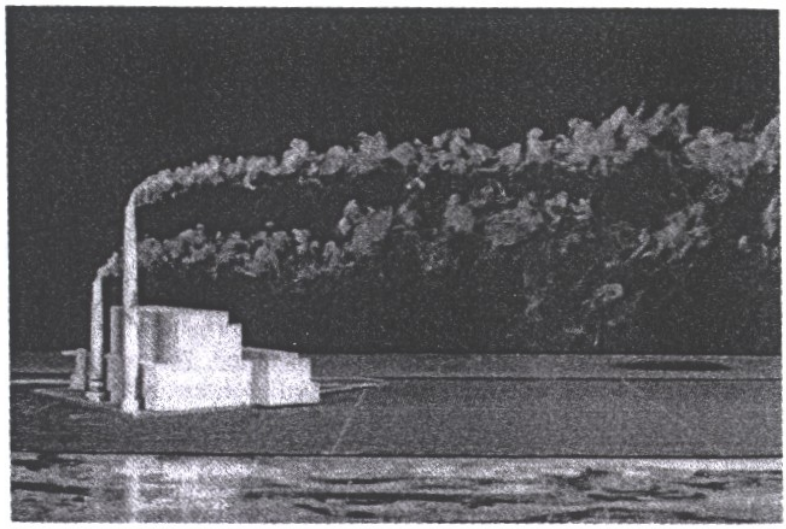

FIGURE 4-11 Perturbation of stack plumes by buildings. Note the effect of increased stack height in eliminating the downwash in the lee of the building. (Courtesy of Professor Gordon Strom.)

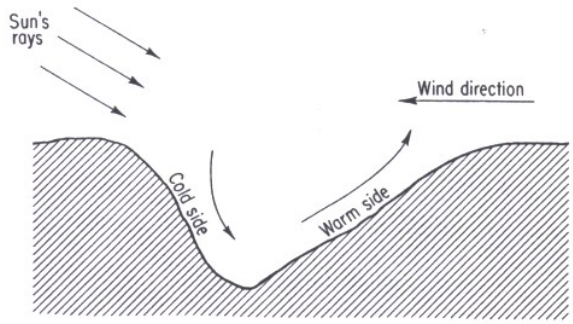

FIGURE 4-15 Atmospheric overturn caused by uneven solar heating of valley walls. [From U.S. Weather Bureau (1955).]